Effect of maturation on the bulk optical properties of apple skin and cortex in the 500 to 1850 nm wavelength range

Robbe Van Beers [a,*], Ben Aernouts [a,b], Rodrigo Watté [a], Ann Schenk [c], Bart Nicolaï [a,c], Wouter Saeys [a]

[a] KU Leuven Department of Biosystems, MeBioS, Kasteelpark Arenberg 30, 3001 Leuven, Belgium
[b] KU Leuven Department of Microbial and Molecular Systems, Cluster for Bioengineering Technology, Campus Geel, Kleinhoefstraat 4, 2440 Geel, Belgium
[c] VCBT - Flanders Centre of Postharvest Technology, Willem de Croylaan 42, 3001 Leuven, Belgium
** Email: wouter.saeys@kuleuven.be*
Tel: +32 (0) 16 37 71 32
Fax: +32 (0) 16 32 19 94

Abstract

To facilitate the design of new optical measurement systems for biological systems, the knowledge of light propagation properties is essential. Therefore, the bulk optical properties of skin and cortex of three apple cultivars were studied during maturation, in the 500 nm to 1850 nm range. A clear absorption signature was observed with absorption peaks which can be related to present anthocyanins, chlorophyll, carotenoids and water. During maturation, the skin absorption at 550 nm increased in the bicolored cultivars '*Braeburn*' and '*Kanzi*', while the absorption at 680 nm decreased in the cortex. Both the bulk scattering coefficient and the anisotropy factor were larger for the skin compared to the cortex tissue. Also during maturation, the skin scattering increased in the two bicolored cultivars, while a general decrease was seen in the apple cortex. Physiological changes during maturation, like cell growth, the formation/degradation of pigments and the formation of a cuticle layer on the skin, may explain the observed evolutions. As a result, using the bulk optical properties, these physiological changes can be monitored and linked to the maturity stage in the orchard, supporting the selective harvest of apples.

Keywords: Apple, Double Integrating Spheres, Unscattered transmittance, Absorption, Scattering, Anisotropy factor

1. Introduction

Optical measurement techniques like visible (vis) and near-infrared (NIR) spectroscopy (Nicolaï et al., 2014), hyperspectral imaging (Boldrini et al., 2012), spatially resolved spectroscopy (Van Beers et al., 2015) and time resolved spectroscopy (Torricelli et al., 2013) have shown to be valuable for the nondestructive quality measurement of different types of intact fruits. Photons entering a material can be absorbed by the molecular bonds, or scattered at mismatches in the refractive index within the turbid product. The absorption, therefore, refers to the chemical properties of the material, while the scattering of photons is related to the (micro)structure (Renfu Lu, 2004). Firmness, crispiness and mealiness are important fruit quality properties which are associated with the microstructure of the apple cortex. As the latter influences the light propagation through the tissue, these properties might be extracted from the signals measured by optical sensors. Yet, in non-destructive measurements, the photons will first have travelled through the pigmented skin layer before reaching the apple cortex (Saeys et al., 2008), therefore influencing the obtained signal. Consequently, the signals measured by optical systems contain information on absorption and scattering of both the apple skin and cortex. Thus, the correlation between quality parameters and the optical output is generally based on chemical and physical attributes of both layers, which complicates the construction and interpretation of calibration models. Therefore, the optical properties of both apple skin and cortex should be better understood, to allow light propagation models to be used as a tool for the development of new optical measurement techniques.

The propagation of light in turbid media, like biological materials, can be described using the bulk optical properties (BOP): the bulk absorption coefficient μ_a, the bulk scattering coefficient μ_s and the angular scattering pattern, represented by the normalized scattering phase function $p(\theta)$ (Aernouts et al., 2014). The phase function describes the normalized scattering probability as a function of the scattering angle θ. However, this function is often too complex to interpret and is, therefore, represented by the anisotropy factor g, which equals the mean cosine of the scattering angle (Aernouts et al., 2013). The wavelength dependent scattering direction of vis/NIR light in biological tissues can often be described with an anisotropy factor in-between isotropic Rayleigh scattering (g = 0) and complete forward scattering (g = 1) (Aernouts et al., 2015). The reduced scattering coefficient μ_s' combines the bulk scattering coefficient and the anisotropy factor into a single parameter, which is sufficient to describe light scattering in the diffusion regime (Tuchin, 2007).

Several researchers have tried to estimate the bulk optical properties of apple tissues with non-destructive optical measurement techniques such as spatially resolved spectroscopy (Cen et al., 2013; Nguyen Do Trong et al., 2014; Qin et al., 2009; Qin & Lu, 2008) or time resolved spectroscopy (Cubeddu et al., 2001; Seifert et al., 2014), in combination with inverse light propagation models (Torricelli et al., 2013). However, it is difficult to estimate the properties of both skin and flesh simultaneously from such measurements. Moreover, most studies on apples focused on the estimation of μ_a and μ_s' (Cen et al., 2013; Lu et al., 2010; Rowe et al., 2014), while less attention has been given to the actual bulk scattering coefficient μ_s and the scattering anisotropy g. If *in vitro* characterization of a thin (mm-range) homogeneous sample slab is feasible, the total reflectance and transmittance can be measured with integrating spheres, generally accepted as the 'golden standard' method to estimate BOP for biological tissues (Aernouts et al., 2013; Bashkatov et al., 2005; López-Maestresalas et al., 2015; Rowe et al., 2014; Saeys et al., 2008; Zamora-Rojas et al., 2013). Moreover, this technique allows to measure BOP of separate tissue layers. In addition, if the BOP can be monitored during maturation, changes in the measured BOP could be related to

physiological changes during this period. This would enable the design of non-destructive optical measurement techniques to monitor apple maturity, supporting the selective harvest and an accurate harvest time prediction.

Therefore, in this research, the evolution of the bulk optical properties (BOP) of apple skin and cortex were studied during maturation, as well as their relation with relevant apple quality and ripeness indicators. Three different apple cultivars, two bicolored (*'Braeburn'* and *'Kanzi'*) and one green cultivar (*'Greenstar'*), were tested. Reliable double integrating sphere (DIS) and unscattered transmittance (UT) measurements were used to obtain accurate estimates for the bulk absorption coefficient μ_a, the bulk scattering coefficient μ_s and the scattering anisotropy factor *g*.

2. Materials and methods

2.1 Apple samples

Apples of the cultivars *'Braeburn'*, '*Kanzi'* and *'Greenstar'* were harvested during the 2014 season in Belgium over a timespan ranging from 45 d before to 17 d after the start of the optimal harvest window. All apples were freshly picked at the 'Centre Fruitier Wallon' in Merdorp, Belgium (50°38'32.7"N 5°00'13.6"E) on the day of the optical measurements. Due to the experimental nature of this orchard, not all apples were removed from the tree in the determined harvest window, and apples were still available for picking until 17 d after the harvest window started. The Belgian harvest windows for the different cultivars were determined by the Flanders Centre for Postharvest Technology (VCBT) based on the evolution of firmness, starch index, soluble solids content (SSC), acidity, size, background color and Streif index after comparing them to historical records (Peirs et al., 2005). Due to differences in the harvest window between cultivars, not all apples were measured over the

exact same time span. Weekly, 5 apples per cultivar were harvested in the mid-section of the tree. Accordingly, a total of 50 *'Braeburn'* apples, 35 *'Kanzi'* apples and 40 *'Greenstar'* apples were picked and the BOP of the skin and fruit cortex were measured.

Parallel to the optical characterization of apple skin and cortex, additional apples of the same cultivars and location were harvested for destructive analysis on the same days. The SSC (°Brix) of the apple juice was measured using a digital refractometer (PR-101α, Atago, Tokyo, Japan). As a measure of apple firmness, the maximum force to puncture the apple for 8 mm using an 11 mm diameter plunger at 8 mm/s was determined using a universal testing machine (LRX, LLOYD Instruments Ltd., Hampshire, UK) (Van Beers et al., 2015). The SSC and firmness were determined on a set of 20 apples per picking date, while for the starch conversion value a different set of 10 apples was used, to ensure this measurement was performed as close as possible to the moment of harvest (Peirs et al., 2005). The starch conversion value was determined using a starch conversion chart (scale from 1 to 10, Ctifl, Paris, France). After performing a Lugol's test, which stains the present starch particles using a KI/I_2 solution on equatorially cut apples, the resulting staining pattern was visually compared to the chart. Based on the discoloration over the entire surface, a score between 1, a high discoloration, and 10, a low discoloration, was defined (Peirs et al. 2002). All these parameters were measured by the Flanders Centre for Postharvest Technology (VCBT) according to the ISO/IEC 17025 standard.

2.2 Sample preparation

Both apple skin and cortex samples were optically characterized on the sun exposed side (blush side), resulting in two measurements per apple. As this side is exposed, it is most interesting for future field measurements. To only obtain the apple skin, first a slice of 6 mm in thickness was cut from the apple using a meat slicer (Junior sup 19 mod 30-595A, CAD, Italy). After this, the excess fruit cortex was scraped off using a scalpel. This remaining skin layer essentially consisted of the cutin layer plus the epicuticular wax, the epidermis and probably also some layers of hypodermis cells. Next, these skin samples were cut into disks

of 30 mm in diameter and placed in a glass cuvette. The custom-made glass cuvette consisted of two parallel 1.1 mm thick glass plates (Borofloat33, Schott, Germany) separated by a spacer of 0.55 mm in thickness. This spacer had a round hole with a diameter of 30 mm. By putting the sample in the provided space, the sample was positioned between the two 1.1 mm glass plates. As the apple skin samples were typically thinner than 0.55 mm, demineralized water was added to remove any unwanted air bubbles and to reduce the refractive index mismatches at the boundaries between the glass plates and the sample. The apple cortex samples were obtained by slicing the apple at the same place where the skin sample was removed. The same meat slicer was used to slice the apple cortex to a thickness of about 0.50 mm. These slices were again loaded in a similar custom made glass cuvette after which demineralized water was added. For both the apple skin and cortex samples, the thickness was measured in triplicate using a digital caliper before loading the samples into the glass cuvette. Also, if obvious defects in one of the samples (e.g. cracks, air bubbles,…) occurred, this sample was not measured and a new sample was prepared.

Once the samples were prepared, the glass cuvette was placed into the sample holder between the double integrating spheres to measure the total reflectance and transmittance. All samples were measured directly after preparation, by which drying and browning effects due to enzymatic reactions were minimized. Repositioning of the sample in a different measurement path allowed to measure the unscattered transmittance (Aernouts et al., 2013).

2.3 Double integrating spheres and unscattered transmittance measurement

The measurement setup used in this research has been described in detail by Aernouts et al. (2013). In brief, a supercontinuum laser (SC450-4, Fianium Ltd., Southampton, UK) with a total output power of 4 W and a spectral broadening over the range 450-2400 nm was used as a light source. By combining this laser light source with a monochromator (Oriel Cornerstone 260 ¼ m, Newport, Irvine, USA), a monochrome tunable light beam was obtained. In this research, the wavelength of the illuminating beam was scanned from 500 nm to 1850 nm, with an interval step of 5 nm. During the optical measurements, 10% of the

light beam leaving the monochromator was collected by reference detectors to monitor the stability of the system. For this, a Si detector (PDA100A, Thorlabs Inc., New Jersey, USA) and a one-stage Peltier-cooled extended-InGaAS detector (PDA10DT-EC, Thorlabs Inc., New Jersey, USA) were used for wavelengths below and above 1050 nm, respectively. Using a flip mirror, the remaining 90% of the monochrome light beam was guided to either the DIS or the unscattered transmittance measurement path.

The DIS measurement path was used to determine the total reflectance (M_R) and the total transmittance (M_T) of the sample. For this, the sample was placed in a sample holder positioned between two *Infragold*® coated integrating spheres (RT-060-IG, Labsphere Inc., North Sutton, USA): one sphere to measure the total reflectance and one sphere to measure the total transmittance. Both a Si and extended-InGaAS detector were mounted on each sphere to measure the obtained diffuse signal over the entire wavelength range from 500 nm to 1850 nm. The unscattered transmittance (M_U) was measured in a separate measurement path where the sample was placed in an identical sample holder located perpendicular to the incident collimated light beam (Aernouts et al., 2013). Two detectors, Si and extended-InGaAs, were placed at a distance of 1.5 m behind the sample to minimize the number of measured scattered photons.

All the detectors in the setup were read by a data acquisition card (NI PCI-6251, National Instruments Corporation, Texas, USA), while the measurement procedure was programmed in LabView 8.5 (National Instruments Corporation, Austin, TX, USA) (Aernouts et al., 2013).

2.4 Bulk Optical Properties estimation

After measuring M_R, M_T and M_U using the DIS and unscattered transmittance measurements, the BOP were estimated using the inverse adding-doubling (IAD) program developed and optimized by Prahl et al. (1993). To use this inverse estimation code, several setup and sample related parameters have to be provided to the software. More details on the setup related parameters, like sphere wall efficiency, diameter of the light spot, refractive index of

188 the cuvette windows, etc. can be found in Aernouts et al. (2013). Another required parameter
189 is the sample's refractive index, which is expected to be close to the one of water as it is the
190 most important chemical component in apple tissue. Moreover, the wavelength-dependent
191 real refractive index of water from Hale & Querry (1973) was used and a wavelength-
192 independent constant was added. Saeys et al. (2008) used a refractive index of 1.37 at 589.3
193 nm, while the refractive index of water at this wavelength is 1.33 (Hale & Querry, 1973).
194 Therefore, based on these findings, a constant of 0.04 was added to the wavelength-
195 dependent refractive index of water for both apple skin and cortex.

196 ### *2.5 Data Processing*

197 The BOP values were calculated considering the entire sample cuvette thickness of 0.55
198 mm. As the samples were not filling the entire cuvette space, a correction had to be made
199 according to the thickness of the used sample. The mean sample thicknesses of three
200 repetitions are listed per cultivar in Table 1. As can be seen, the thickness of the apple skin is
201 not the same for the different cultivars, while the apple cortex samples were sliced to be
202 uniform in thickness, independent of the cultivar.

203 **Table 1 Mean thicknesses with standard deviation of the measured apple skin and cortex samples**

	Skin (mm)	Cortex (mm)
Braeburn	0.213 ± 0.022	0.497 ± 0.035
Kanzi	0.291 ± 0.033	0.497 ± 0.039
Greenstar	0.225 ± 0.024	0.516 ± 0.039

204

205 Knowing the sample thickness, the following equations were used to perform a sample
206 specific thickness correction for both the bulk absorption coefficient (μ_a) and the reduced
207 scattering coefficient (μ_s') separately:

208 $$\mu_{a,corrected} = \left(\mu_{a,calculated} - \mu_{a,water} \frac{d_{water}}{d_{total}} \right) \frac{d_{total}}{d_{sample}} \quad (1)$$

$$\mu'_{s,corrected} = \mu'_{s,calculated} \frac{d_{total}}{d_{sample}} \quad (2)$$

Equation (1) shows the thickness correction for μ_a, while equation (2) shows the correction performed for μ_s'. In these equations, the assumption was made that a perfect two-layered system was obtained with one layer being the sample and the other being water. In both equations, d stands for the thickness of the different layers, where the total thickness (d_{total}) corresponds to 0.55 mm. For the correction of the absorption coefficient, the absorption coefficient of water ($\mu_{a,water}$) was measured in the unscattered transmittance path using the same cuvette. As water does not scatter light, the (reduced) scattering coefficient only had to be corrected for the thickness of the sample (d_{sample}). The anisotropy factor did not require a correction as it is independent of the actual sample thickness. Finally, the bulk scattering coefficient μ_s was derived from μ_s' and g through the similarity relation (Tuchin, 2007):

$$\mu_s = \frac{\mu'_s}{(1-g)} \quad (3)$$

3. Results

3.1 Apple maturation

In Figure 1a to Figure 1c the evolution of three maturity related parameters (SSC, firmness and starch conversion) is illustrated for the entire measuring period from 45 d before to 17 d after the moment of optimal harvest. The evolution of the Streif index, a maturity index combining these three maturity related parameters, is shown in Figure 1d (Streif, 1996; Van Beers et al., 2015).

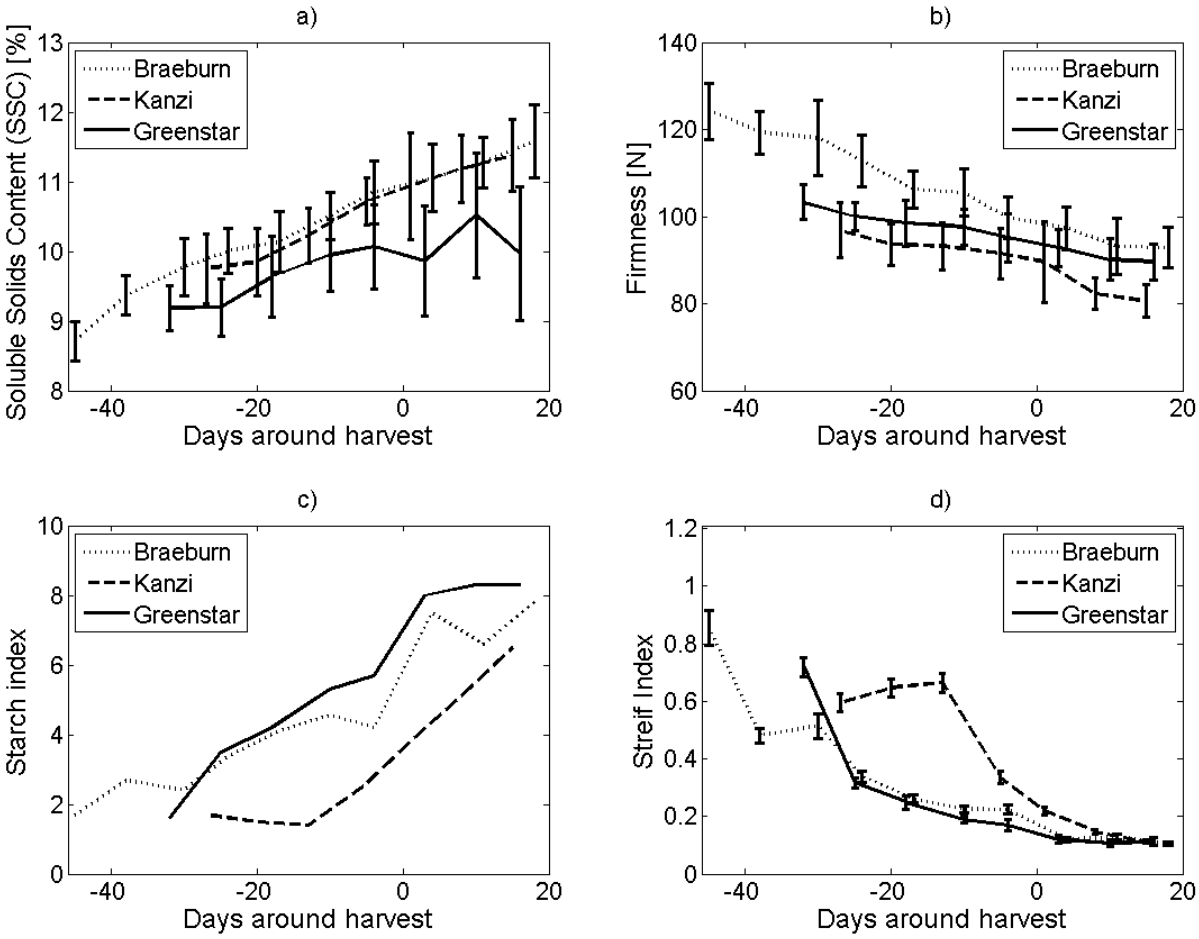

230

231 **Fig. 1** The evolution of (a) soluble solids content, (b) firmness, (c) starch conversion values
232 and (d) the Streif index, a combination of the parameters in (a)-(b)-(c), during apple fruit
233 maturation. The error bars indicate the observed standard deviation.
234

235 Several characteristic trends during maturation can be observed in Figure 1: the SSC values
236 (Figure 1a) and starch index (Figure 1c) increase, while the firmness values (Figure 1b) and
237 the Streif index (Figure 1d) decrease. However, all measured parameters are location and
238 cultivar specific (Peirs et al., 2001). During maturation, the Streif index generally shows a
239 sigmoidal trend towards the moment of harvest. This index is often used as a maturity
240 parameter which indicates the appropriate time to harvest when it drops below a cultivar
241 specific threshold.

242

243

3.2 Bulk optical properties of three apple cultivars

In Figure 2 the mean estimated bulk absorption coefficient spectra calculated over four weeks around harvest (20 apples) are shown for both the apple skin (Figure 2a) and the apple cortex (Figure 2b) for the three measured apple cultivars. Absorption peaks at 550 nm and 680 nm occur in the visible part of the spectrum, at which the three cultivars showed clear differences in absorption. The absorption at 680 nm in the skin tissue (Figure 2a) is highest in the green cultivar *'Greenstar'*, with a mean value up to 16.5 cm^{-1}. *'Kanzi'* has the lowest absorption at this wavelength with a mean value of 6.9 cm^{-1}. Compared to the skin, the cortex absorption at 680 nm is much lower with mean values up to 0.4 cm^{-1} for *'Greenstar'* (inset of Figure 2b). At a wavelength of 550 nm, a high absorption was observed for the bicolored cultivars *'Braeburn'* and *'Kanzi'*. Other absorption peaks were present in the NIR part of the spectrum, at 970 nm, 1200 nm and 1450 nm.

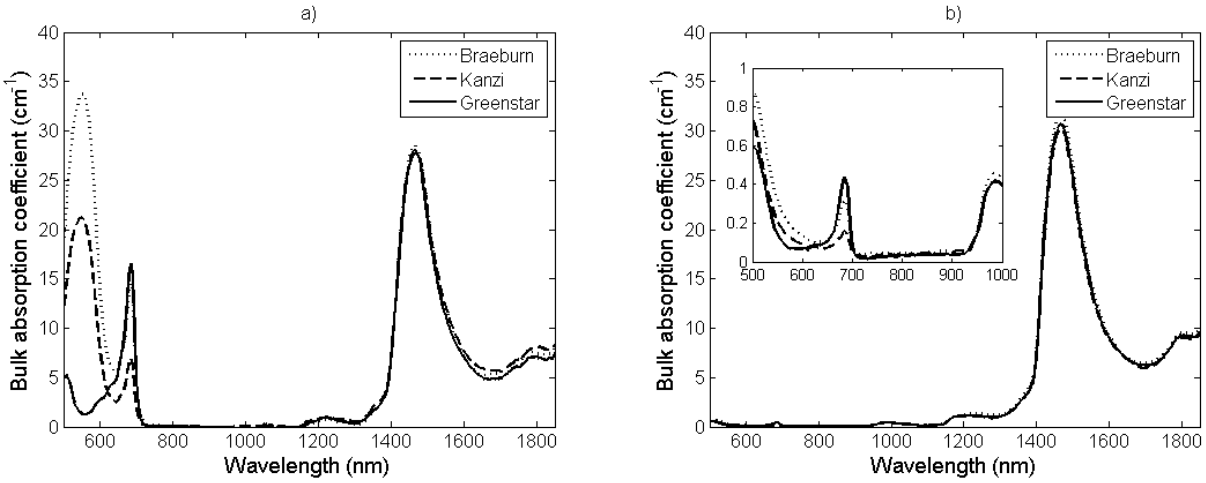

Fig. 2 Mean bulk absorption coefficient μ_a spectra for (a) the skin and (b) the cortex tissue of three apple cultivars during four weeks around harvest. The inset figure shows the absorption coefficient spectra for apple cortex in the 500-1000 nm range.

In Figure 3, the mean measured reduced scattering coefficient (μ_s') spectra during four weeks around harvest are visualized for both apple skin (Figure 3a) and cortex (Figure 3b). It is clear from Figure 3 that the reduced scattering coefficient decreases exponentially with increasing wavelength, which is typical for biological tissues (Bashkatov et al., 2005). This evolution is more pronounced in the apple skin compared to the apple cortex, especially in

the visible region of the spectrum. Moreover, a flatter course is seen for the μ_s' spectra of apple cortex with values around 10 cm^{-1}. Some small cultivar differences are present in both the skin and cortex tissue. Especially the *'Braeburn'* cultivar shows a difference over the entire wavelength range, where the μ_s' of the skin is higher compared to the other cultivars, while for the apple cortex it is lower. For *'Greenstar'*, the μ_s' values of the skin and cortex were similar for wavelengths above 1000 nm. Moreover, in this region, the reduced scattering coefficient of *'Kanzi'* cortex is even higher than that of the skin.

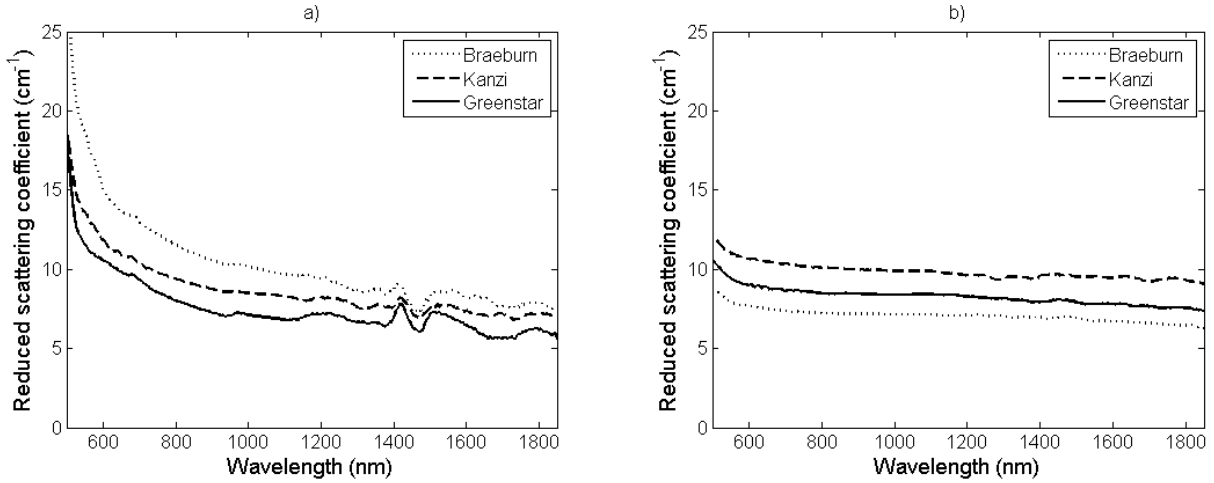

Fig. 3 Mean reduced scattering coefficient μ_s' of (a) apple skin and (b) cortex tissue of three apple cultivars during four weeks around harvest.

The accurate measurement of the unscattered transmittance in this study resulted in a robust estimation of both the bulk scattering coefficient μ_s (Figure 4a) and the anisotropy factor *g* (Figure 4b).

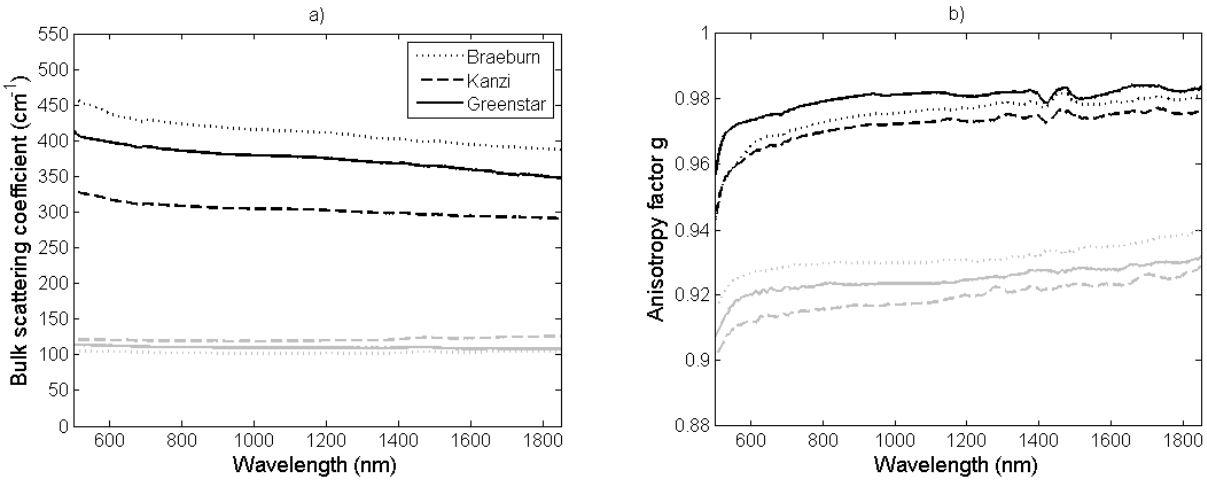

Fig. 4 (a) Mean bulk scattering coefficient μ_s and (b) anisotropy factor g of both the skin (black lines) and cortex tissue (grey lines) of three apple cultivars during four weeks around harvest.

In Figure 4, a clear difference can be noticed between the scattering properties of apple skin (black lines) and cortex (grey lines). The μ_s of the skin decreases with increasing wavelength, while the μ_s of the cortex is more wavelength independent. The anisotropy factor of both the apple skin and cortex shows an increase with increasing wavelength, typical for biological tissues (Jacques, 2013). The apple skin samples have a high bulk scattering coefficient, with mean values up to 425 cm^{-1} at 800 nm. This is significantly higher than for the apple cortex, which has mean values up to 120 cm^{-1} at the same wavelength. When comparing the three different cultivars, *'Kanzi'* differs the most from the other two cultivars. The μ_s of the skin is significantly lower, with a value of 308 cm^{-1} at 800 nm, compared to 386 cm^{-1} and 423 cm^{-1} for *'Greenstar'* and *'Braeburn'*, respectively. For the cortex samples, an opposite trend can be noticed, as *'Kanzi'* shows the highest μ_s, going up to 119 cm^{-1} at 800 nm.

Similar to the bulk scattering coefficient, a significant difference in the anisotropy factor (g) between apple skin and cortex can be observed in Figure 4b. Both apple skin and cortex have an anisotropy factor close to one, which indicates a high forward scattering. The results indicate that the apple skin is more forward scattering compared to the cortex, with a g-value at 800 nm of 0.97 for the skin compared to 0.93 for the cortex.

3.3 Evolution of optical properties during maturation

3.3.1 Absorption properties

In Figure 5, the evolution of the apple skin's bulk absorption coefficient (μ_a) at 550 nm over the measured maturation period is illustrated. The solid lines indicate the observed trends in the three different apple cultivars, while the error bars indicate the corresponding standard deviations.

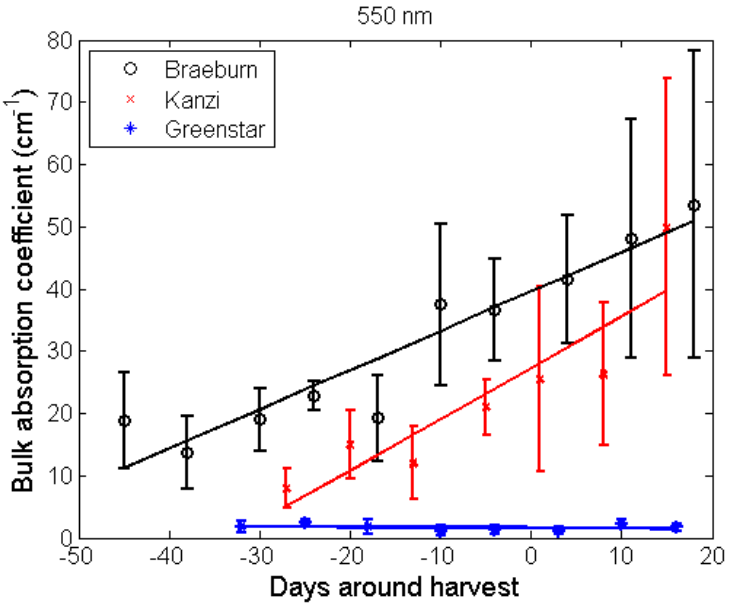

Fig. 5 Bulk absorption coefficient at 550 nm during maturation for the skin of three apple cultivars. The error bars indicate the standard deviation.

From Figure 5 it can be observed that the absorption coefficient values at 550 nm for the skin samples increased significantly ($p<0.01$) towards the moment of harvest (and afterwards) in *'Braeburn'* and *'Kanzi'* apple cultivars. A large standard deviation can be observed for both red cultivars, while the *'Greenstar'* cultivar shows much lower variations. Moreover, no significant increase in the absorption at 550 nm was seen in this green cultivar.

The evolution of the absorption coefficient at 680 nm is shown in Figure 6 for both the apple skin (Figure 6a) and cortex (Figure 6b).

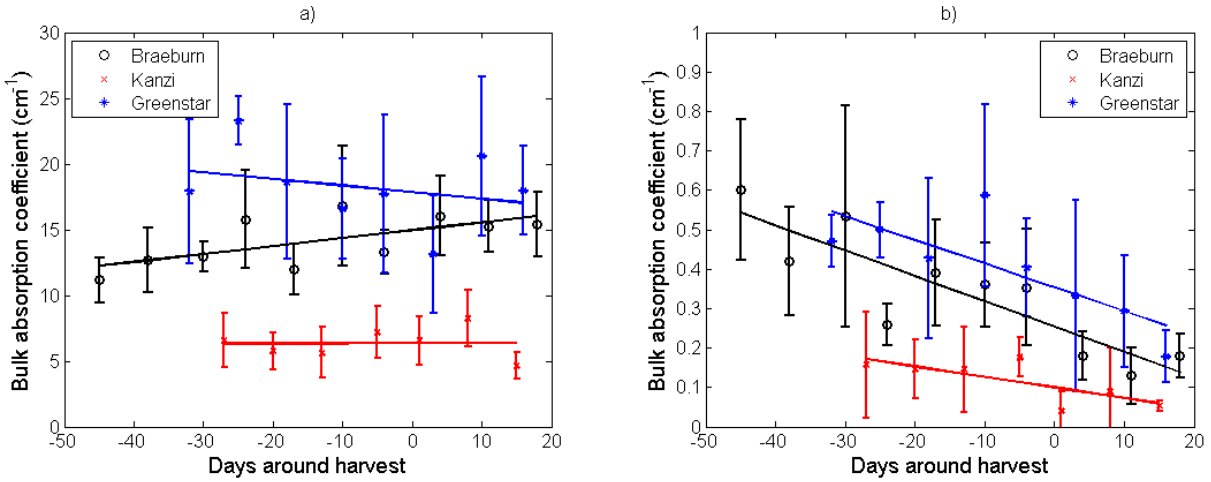

Fig. 6 Bulk absorption coefficient at 680 nm during maturation for both (a) the skin and (b) cortex of three apple cultivars. The error bars indicate the standard deviation.

While a clear upwards evolution in the skin absorption at 550 nm could be observed for *'Kanzi'* and *'Braeburn'*, the change in absorption by the skin at 680 nm is much less obvious (Figure 6a). Only a significant change ($p<0.01$) was found for *'Braeburn'* skin samples. Although non-significant ($p=0.331$), *'Greenstar'* showed a slightly decreasing trend (Figure 6a). In the apple cortex, a significant downward trend in the μ_a at 680 nm was observed in both *'Kanzi'* ($p<0.05$) and *'Greenstar'* ($p<0.01$). *'Braeburn'* also showed this downwards trend in Figure 6b, but the observed trend was not statistically significant ($p=0.0664$).

3.3.2 Scattering properties

In Figure 7 and Figure 8 the evolution of the bulk scattering coefficient μ_s and the scattering anisotropy factor g during maturation is illustrated. The scattering trends are shown for one specific wavelength (850 nm), as both μ_s and g are mostly wavelength-independent for wavelengths above 700 nm.

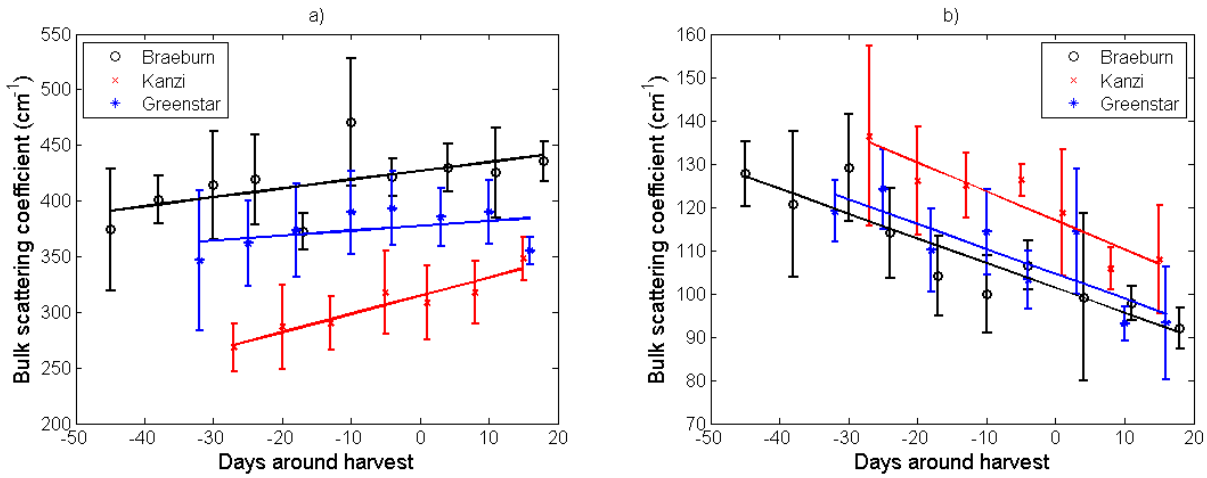

Fig. 7 Bulk scattering coefficient at 850 nm during maturation for both (a) the skin and (b) the cortex of three apple cultivars. The error bars indicate the obtained standard deviation.

In Figure 7a, an upward trend in the skin's bulk scattering coefficient with maturation can be observed, while a downward trend is observed for the apple cortex (Figure 7b). All of these trends were significant ($p<0.05$) except for *'Greenstar'* skin. In *'Greenstar'* skin, first an increase is noticed, while around harvest, the values start to decrease.

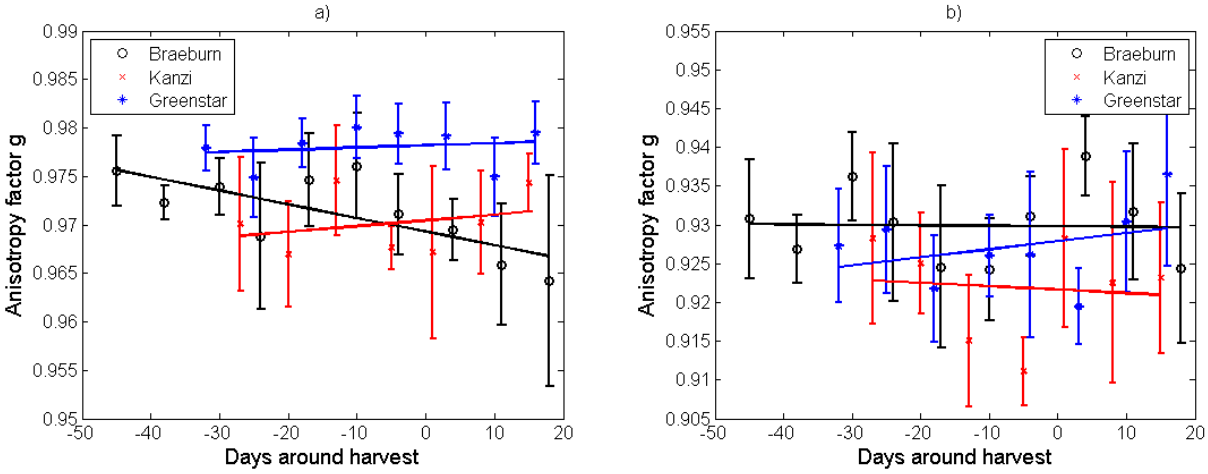

Fig. 8 Anisotropy factor *g* at 850 nm during maturation for both (a) the skin and (b) the cortex of three apple cultivars. The error bars indicate the obtained standard deviation.

Figure 8 indicates that, during maturation, no consistent evolutions in the anisotropy factor could be observed for the apple skin and cortex for any of the three cultivars. Only a significant change ($p<0.01$) was noticed in anisotropy factor for the apple skin of *'Braeburn'*

apples. This decreasing trend is mainly present after the optimal point of harvest, whereas before this point no large change could be observed.

Finally, the trends for the reduced scattering coefficient μ_s' during maturation were studied as well (figure not shown). This coefficient is a combination of μ_s and g (equation (3)) and therefore shows a combined effect of both parameters. Like μ_s, the reduced scattering coefficients of the fruit cortex showed a significant downwards trend ($p<0.05$) for all cultivars. However, in the apple skin, only a significantly increasing trend was observed in *'Braeburn'*.

4. Discussion

4.1 Apple bulk optical properties

Figure 2 illustrated the main absorption peaks for both the apple skin and cortex. Based on literature, these absorption peaks are most likely related to the presence of carotenoids (around 500 nm), anthocyanins (550 nm – 600 nm), chlorophyll (mainly *chlorophyll a* at 678 nm) and water (Lancaster et al., 1994; Merzlyak et al., 2003). The most important anthocyanin responsible for the red apple color is cyanidin 3-*O*-galactoside (Espley et al., 2007; Lancaster et al., 1994), while known carotenoids in the apple skin are lutein, violaxanthin, neoxanthin and β-carotene (Delgado-Pelayo et al., 2014). While carotenoids, anthocyanins and chlorophyll are the main pigments in the apple skin, also the cortex μ_a spectra contained features related to the presence of chlorophyll and carotenoids (inset in Figure 2b). From literature, water is known to have prominent absorption peaks in the NIR part of the spectrum, respectively at 970 nm, 1200 nm and 1450 nm (Hale & Querry,1973). Lipids in the cuticular wax layer on the apple skin can absorb light in the region around 1200 nm (Veraverbeke et al., 2005).

As *'Greenstar'* is a green cultivar, very little anthocyanins are formed in the apple skin, which could explain the low absorption at 550 nm. In contrast, both bicolored cultivars (*'Kanzi'* and *'Braeburn'*) showed high absorption at 550 nm with mean values up to 34 cm^{-1} for *'Braeburn'*.

376 Additionally, in the skin of *'Greenstar'* and the cortex of all three cultivars, substantial
377 absorption can be noticed around 500 nm, which might be attributed to the presence of
378 carotenoids (Merzlyak et al., 2003).

379 When comparing the obtained bulk absorption coefficients with the values reported in
380 literature, some differences can be noticed. Cubeddu et al. (2001) found a maximal
381 absorption coefficient at 680 nm of 0.25 cm^{-1} in *'Granny Smith'* using time resolved
382 spectroscopy. With spatially resolved spectroscopy, maximal chlorophyll peaks of 0.6 cm^{-1}
383 and 2.5 cm^{-1} were obtained in *'Golden Delicious'* and *'Braeburn'* apples respectively (Nguyen
384 Do Trong et al., 2014; Qin & Lu, 2008). However, these techniques measured the whole
385 apple, with the former penetrating deeper than the latter, therefore showing the bulk effect of
386 both the skin and cortex absorption in a different ratio. Moreover, the estimation of optical
387 properties involves modeling the light propagation into the tissue using Monte Carlo
388 simulations (Qin & Lu, 2009), the diffusion approximation of the radiative transfer equation
389 (Cubeddu et al., 2001) or a metamodeling approach (Aernouts et al., 2015; Nguyen Do
390 Trong et al., 2014). Therefore, the obtained BOP also depend on the viability and robustness
391 of the used modeling approaches, as well as on the assumptions made by these techniques.
392 For the estimation of the BOP of apple, both Saeys et al. (2008) and Rowe et al. (2014) used
393 a single integrating sphere measurement. Like the results obtained in this research, Saeys et
394 al. (2008) found a μ_a around 680 nm between 5 and 10 cm^{-1} for *'Braeburn'* apple skin, while
395 higher absorption values up to 30 cm^{-1} were observed at a wavelength of 500 nm. For the
396 apple cortex, mainly water peaks were noticed, while no clear absorption peaks were present
397 in the visible region of the spectrum (Saeys et al., 2008). However, similar to what was seen
398 in Figure 2, Rowe et al. (2014) found an absorption peak at 680 nm of about 0.1 cm^{-1} in the
399 cortex of *Royal Gala* apples at commercial maturity.

400 The obtained reduced scattering coefficients in Figure 3 were consistent with the values
401 reported in literature. Other researchers found μ_s' values for different cultivars ranging
402 between 10 cm^{-1} and 20 cm^{-1} (Cen et al., 2013; Cubeddu et al., 2001; Nguyen Do Trong et

al., 2014; Qin & Lu, 2008; Rowe et al., 2014; Saeys et al., 2008; Seifert et al., 2014). When looking at the skin and cortex tissue separately, Saeys et al. (2008) found a larger μ_s' for skin tissue with values up to 40 cm^{-1} at 600 nm, calculated with a fixed anisotropy factor.

The bulk scattering coefficient μ_s showed clear differences between the apple skin and cortex tissue (Figure 4a), which might be attributed to the cell structure in both tissue types. It was found by other researchers that the apple cortex cells are much larger than the compact epidermis cells (Herremans et al., 2013; Schotsmans et al., 2004; Bain & Robertson, 1951). Moreover, the large cortex cells are separated by big air pores, causing a more spacious structure (Herremans et al., 2013). Consequently, the smaller epidermis and hypodermis cells (Verboven et al., 2008, 2013) have a denser concentration of scattering particles. This cell size difference between the cortex and skin tissue could also explain the steeper decreasing trend in the skin samples, as according to Mie scattering theory this is typically related to smaller scatterers (Aernouts et al., 2015). Saeys et al. (2008) also reported differences between the scattering coefficient of apple skin and cortex, but the actual values were considerably smaller, with a μ_s for skin ranging between 100 cm^{-1} and 150 cm^{-1}, while the μ_s for apple cortex ranged from 30 cm^{-1} to 50 cm^{-1}. The suboptimal configuration for unscattered transmittance measurements used in that study, most likely resulted in the detection of scattered photons and consequently an underestimation of the extinction by the sample (Aernouts et al., 2013). This is most likely the reason why μ_s and g were underestimated in the study of Saeys et al. (2008).

The observed differences in the anisotropy factor g of skin and cortex (Figure 4b) may be attributed to differences in the main scattering particles. The higher g values for the skin samples suggest larger scattering particle sizes. Contradictory, the steeper descend of the skin's bulk scattering coefficient observed earlier would indicate the presence of mainly small scattering particles. However, the Mie scattering theory assumes spherical scattering particles (Aernouts et al., 2015), while many of the scattering particles in plant cells are far from spherical (Konarska, 2014; Stevenson et al., 2006; Verboven et al., 2013). This could

possibly be the reason why the observed relation between the bulk scattering coefficient and anisotropy factor spectra was not consistent with the Mie theory. Saeys et al. (2008) also found that the anisotropy factor of the apple skin was higher compared to the apple cortex. Moreover, Baranyai et al. (2009) found anisotropy factor values around 0.95 at 785 nm during cool storage of *'Pinova'* and *'Elstar'* apples.

4.2 Evolution of optical properties during maturation

To monitor μ_a during maturation, two wavelengths, 550 nm and 680 nm, were followed, because these have been reported to correspond to the absorption peaks of anthocyanins and chlorophyll, respectively (Lancaster et al., 1994; Merzlyak et al., 2003). In Figure 5, showing the evolution of the absorption at 550 nm, a large standard deviation can be observed. This is probably a result of the high variation in anthocyanin concentrations in apple skin (Singha et al., 1991). However, the observations made are in line with other publications on the increase of the anthocyanin concentration during maturation (Awad et al., 2001; Lister et al., 1996; Reay et al., 1998). Furthermore, several researchers have suggested a decrease in the chlorophyll concentration during maturation (McGlone et al., 2002; Mir et al., 2001; Reay et al., 1998; Rutkowski et al., 2008; Song et al., 1997). In Figure 6, showing the absorption at 680 nm during maturation, no significant trends can be observed for the skin samples, except for a significant upward trend in the skin samples of the *'Braeburn'* cultivar. However, for the cortex samples of all three cultivars a significant decreasing trend can be observed.

The scattering of light passing through apple tissue is caused by the scattering particles present, such as cell walls, air pores and cellular content (e.g. vacuoles, starch granules, chloroplasts) (Lu, 2004; Nicolaï et al., 2014; Rowe et al., 2014). For the apple cortex samples of all three cultivars the bulk scattering coefficient values at 850 nm, shown in Figure 7b, decreased significantly during maturation. A possible explanation for this decrease can be found in the apple development. In a first stage of fruit development, cells are rapidly

456 dividing, while the actual size of the apple does not change much. However, during the
457 maturation period considered in this research, the cell division stops after which the newly
458 differentiated cells start to elongate (Bain & Robertson, 1951; Grierson, 2001; Seifert et al.,
459 2014). During this cell elongation, cells and pores both become larger, but their total number
460 does not change. As an effect, the overall apple diameter increases without the formation of
461 new cells. Therefore, less cell walls and air pores will be encountered by the light on a
462 volume basis. This could explain the decreasing scattering coefficient observed. Moreover,
463 during maturation starch is converted into sugars (Smith et al., 2005) resulting in less starch
464 granules and thus scattering particles in the cortex over time. In the skin, an opposite
465 evolution of the scattering properties was observed over time than the one observed for the
466 cortex (Figure 7a). However, a similar evolution during apple development is observed
467 compared to the fruit flesh, where during this period the cell division ceases, followed by a
468 stage of elongation and flattening of the cells during maturation. However, in contrast to the
469 cortex cells, the epidermal cells excrete a waxy, cutinous material during this elongation
470 stage (Grierson, 2001). This cuticle is a heterogeneous polymer of fatty acids overlaid with a
471 layer of wax in which the epidermal cells are embedded and which can even further develop
472 after harvest (Domínguez et al., 2011; Grierson, 2001). In a study performed by Solovchenko
473 & Merzlyak (2003), the cuticle layer of apples was found to have a significant scattering
474 effect, which was observed as a wavelength dependent increase of the cuticular optical
475 depth. This could be the reason for the increase in the apple skin μ_s during maturation.

476 Finally, the absence of changes in the anisotropy factor *g* observed in Figure 8, could confirm
477 the previous observations made for μ_s. Moreover, it was suggested that cell growth could be
478 responsible for the changes in scattering, as less scatterers will be encountered for a similar
479 volume of fruit, while geometry and size of the scattering particles will most likely be
480 constant. For example, chloroplasts stay present in the epidermal cells during maturation,
481 though changes occur in the concentration of chlorophyll. More in detail, the chloroplasts
482 convert into gerontoplasts, by which also structural modifications of the thylakoid membranes

occur inside the organelle. The envelope of the chloroplast, however, remains intact (Biswal et al., 2011). As a result, the main scattering particles likely remain present and the anisotropy factor remains constant.

4.3 General remarks

One of the requirements for the IAD calculations is that the measured samples are homogeneous (Prahl et al., 1993). However, the measured apple samples can have small irregularities, like air pores, color changes, lenticels, etc. Although this effect on the eventual estimation of BOP is believed to be limited, more complex modelling strategies like the meshed Monte Carlo method (Watté et al., 2015a), could provide an added value here.

Herremans et al. (2013) showed that the cortex cells of *'Braeburn'* apples have an average length of 0.299 mm and a width of 0.2175 mm. As the cortex sample thicknesses were only about 0.5 mm (Table 1), only two to four cell layers were sampled, of which two were probably damaged by the cutting procedure. Therefore, it can be expected that the cutting process might have influenced the obtained results. Nevertheless, according to Mie theory the main scattering particles in the vis/NIR region of the spectrum are the cell organelles (Aernouts et al., 2014). Thus, the measured BOP of the apple cortex samples are expected to be valid. Moreover, as variation was also present in the results of the measured skin samples, which were not cut, the effects of biological variability might have been higher in comparison to the introduced effects of cutting.

The obtained results give valuable information to go towards future applications for fruit quality monitoring. The observed trends in BOP might be related to the observed quality changes in Figure 1. However, more measurements on a large set of samples are essential for building robust calibration models. To achieve this, novel optical measurement techniques should be designed which can measure the BOP in a fast and non-destructive way. Light propagation models can be used for *in silico* design of these techniques and the BOP of apple skin and cortex are essential inputs for this. Simulations based on these models will

enable the development and optimization of both sensors and data processing techniques (Watté et al., 2015a; Watté et al., 2015b). These novel sensors could then be used for the monitoring of fruit quality parameters and would promote the evaluation of fruit maturity for picking decisions in mechanical harvesting applications.

5. Conclusions

The absorption coefficient (μ_a) showed absorption features of carotenoids (500 nm), anthocyanins (550 nm), chlorophyll (678 nm), wax lipids (1200 nm) and water (970 nm, 1200 nm and 1450 nm). Most pigments were present in the apple skin, with a maximal absorption by anthocyanins going up to 50 cm^{-1}. In comparison to the bicolored cultivars *'Braeburn'* and *'Kanzi'*, a larger absorption by chlorophyll was observed in the green cultivar *'Greenstar'*, while nearly no anthocyanin absorption could be observed. During maturation, a significant increase in the absorption by anthocyanins was seen in the skin of bicolored cultivars. In contrast, the absorption by chlorophyll showed no clear changes in the apple skin, while in the apple cortex of *'Kanzi'* and *'Greenstar'* a significant decrease was noticed. A clear difference between the scattering properties of apple skin and cortex was observed. The apple skin was more highly scattering compared to the apple cortex. Both the skin and cortex were found to be highly forward scattering, with respective anisotropy factors of 0.97 and 0.93 at 800 nm. All cultivars showed a decrease in the bulk scattering coefficient of the apple cortex during maturation, while it increased in the apple skin of the *'Kanzi'* and *'Greenstar'* cultivars. While clear changes were seen in the scattering, the anisotropy factor only changed in the skin of *'Braeburn'* apples. Therefore, it was hypothesized that the shape and size of the scattering particles are hardly changing during maturation.

Acknowledgements

This project received funding from the MONALISA project, funded by the Autonomous Province of Bolzano/Bozen in Italy. Robbe Van Beers and Rodrigo Watté were funded by the Institute for the Promotion of Innovation through Science and Technology in Flanders (IWT-Flanders, grants 131777 and 101552). Ben Aernouts was funded as a postdoctoral fellow of the Research Foundation Flanders (FWO, Brussels, Belgium, grant 12K3916N). The authors acknowledge the support of the Flanders Centre of Postharvest Technology (VCBT) and its co-workers Dr. Bert Verlinden, Elfie Dekempeneer, Bert Vandebosch and Sofie Mannaerts.

References

Aernouts, B., Erkinbaev, C., Watté, R., Van Beers, R., Do Trong, N. N., Nicolai, B., & Saeys, W. (2015). Estimation of bulk optical properties of turbid media from hyperspectral scatter imaging measurements: metamodeling approach. *Optics Express*, *23*(20), 26049. doi:10.1364/OE.23.026049

Aernouts, B., Van Beers, R., Watté, R., Huybrechts, T., Jordens, J., Vermeulen, D., Van Gerven, T., Lammertyn, J., & Saeys, W. (2015). Effect of ultrasonic homogenization on the Vis/NIR bulk optical properties of milk. *Colloids and Surfaces B: Biointerfaces*, *126*, 510–519. doi:10.1016/j.colsurfb.2015.01.004

Aernouts, B., Van Beers, R., Watté, R., Huybrechts, T., Lammertyn, J., & Saeys, W. (2015). Visible and near-infrared bulk optical properties of raw milk. *Journal of Dairy Science*, *98*(7), 6727–6738. doi:10.3168/jds.2015-9630

Aernouts, B., Watté, R., Van Beers, R., Delport, F., Merchiers, M., De Block, J., Lammertyn, J., & Saeys, W. (2014). Flexible tool for simulating the bulk optical properties of polydisperse spherical particles in an absorbing host: experimental validation. *Optics Express*, *22*(17), 20223. doi:10.1364/OE.22.020223

Aernouts, B., Zamora-Rojas, E., Van Beers, R., Watté, R., Wang, L., Tsuta, M., Lammertyn, J., & Saeys, W. (2013). Supercontinuum laser based optical characterization of Intralipid® phantoms in the 500-2250 nm range. *Optics Express*, *21*(26), 32450–67. doi:10.1364/OE.21.032450

Awad, M. A., De Jager, A., Van Der Plas, L. H. W., & Van Der Krol, A. R. (2001). Flavonoid and chlorogenic acid changes in skin of “Elstar” and “Jonagold” apples during development and ripening. *Scientia Horticulturae*, *90*(1-2), 69–83. doi:10.1016/S0304-4238(00)00255-7

Awad, M. A., Wagenmakers, P. S., & De Jager, A. (2001). Effects of light on flavonoid and chlorogenic acid levels in the skin of “Jonagold” apples. Scientia Horticulturae, 88(4), 289–298. doi:10.1016/S0304-4238(00)00215-6

Bain, J. M., & Robertson, R. N. (1951). The physiology of growth in apple fruits. I. Cell size, cell number, and fruit development. *Australian Journal of Scientific Research. Ser. B: Biological Sciences*, *4*(2), 75–107.

Baranyai, L., Regen, C., & Zude, M. (2009). Monitoring optical properties of apple tissue during cool storage. *Bornimer Agrartechnische Berichte*, (69), 112–119.

Bashkatov, A. N., Genina, É. A., Kochubey, V. I., & Tuchin, V. V. (2005). Optical Properties of the Subcutaneous Adipose Tissue in the Spectral Range 400 – 2500 nm. *Optics and Spectroscopy*, *99*(5), 868–874.

Biswal, B., Mohapatra, P. K., & Biswal, U. C. (2012). Leaf Senescence and Transformation of Chloroplasts to Gerontoplasts. In J. J. Eaton-Rye, B. C. Tripathy, & T. D. Sharkey (Eds.), *Photosynthesis: Plastid Biology, Energy Conversion and Carbon Assimilation, Advances in Photosynthesis and Respiration* (Vol. 34, pp. 217–230). Springer Science+ Business Media B.V. 2012. doi:10.1007/978-94-007-1579-0

581 Boldrini, B., Kessler, W., Rebner, K., & Kessler, R. W. (2012). Hyperspectral imaging: a
582 review of best practice, performance and pitfalls for in-line and on-line applications. *Journal*
583 *of Near Infrared Spectroscopy*, *20*, 483–508. doi:10.1255/1003

584 Cen, H., Lu, R., Mendoza, F., & Beaudry, R. M. (2013). Relationship of the optical absorption
585 and scattering properties with mechanical and structural properties of apple tissue.
586 *Postharvest Biology and Technology*, *85*, 30–38. doi:10.1016/j.postharvbio.2013.04.014

587 Cubeddu, R., D'Andrea, C., Pifferi, A., Taroni, P., Torricelli, A., Valentini, G., Ruiz-Altisent,
588 M., Valero, C., Ortiz, C., Dover, C., & Johnson, D. (2001). Time-Resolved Reflectance
589 Spectroscopy Applied to the Nondestructive Monitoring of the Internal Optical Properties in
590 Apples. *Applied Spectroscopy*, *55*(10), 1368–1374.

591 Domínguez, E., Cuartero, J., & Heredia, A. (2011). An overview on plant cuticle
592 biomechanics. *Plant Science*, *181*(2), 77–84. doi:10.1016/j.plantsci.2011.04.016

593 Delgado-Pelayo, R., Gallardo-Guerrero, L., & Hornero-Méndez, D. (2014). Chlorophyll and
594 carotenoid pigments in the peel and flesh of commercial apple fruit varieties. *Food Research*
595 *International*, 65(PB), 272–281. doi:10.1016/j.foodres.2014.03.025

596 Espley, R. V., Hellens, R. P., Putterill, J., Stevenson, D. E., Kutty-Amma, S., & Allan, A. C.
597 (2007). Red colouration in apple fruit is due to the activity of the MYB transcription factor,
598 MdMYB10. *Plant Journal*, 49(3), 414–427.

599 Grierson, W. (2001). Fruit Development, Maturation, and Ripening. In M. Pessarakli (Ed.),
600 *Handbook of Plant and Crop Physiology* (Second Edi., pp. 143–160). New York, NY: Marcel
601 Dekker, Inc.

602 Hale, G. M., & Querry, M. R. (1973). Optical Constants of Water in the 200-nm to 200-µm
603 Wavelength Region. *Applied Optics*, *12*(3), 555–563. doi:10.1364/AO.12.000555

604 Herremans, E., Verboven, P., Bongaers, E., Estrade, P., Verlinden, B. E., Wevers, M.,
605 Hertog, M., Nicolai, B. M. (2013). Characterisation of "Braeburn" browning disorder by means
606 of X-ray micro-CT. *Postharvest Biology and Technology*, *75*, 114–124.
607 doi:10.1016/j.postharvbio.2012.08.008

608 Jacques, S. L. (2013). Optical Properties of Biological Tissues: A Review. *Physics in*
609 *Medicine and Biology*, *58*(11), R37–61. doi:10.1088/0031-9155/58/11/R37

610 Konarska, A. (2014). Morphological, Histological and Ultrastructural Changes in Fruit
611 Epidermis of Apple Malus Domestica cv. Ligol (Rosaceae) at Fruit Set, Maturity and Storage.
612 *ACTA BIOLOGICA CRACOVIENSIA Series Botanica*, *56*(2), 35–48. doi:10.2478/abcsb-
613 2014-0019

614 Lancaster, J. E., Grant, J. E., Lister, C. E., & Taylor, M. C. (1994). Skin Color in Apples -
615 Influence of Copigmentation and Plastid Pigments on Shade and Darkness of Red Color in
616 Five Genotypes. *Journal of the American Society for Horticultural Science*, *119*(1), 63–69.

617 Lister, C. E., Lancaster, J. E., & Walker, J. R. L. (1996). Developmental changes in enzymes
618 of flavonoid biosynthesis in the skins of red and green apple cultivars. *Journal of the Science*
619 *of Food and Agriculture*, *71*(3), 313–320. doi:10.1002/(SICI)1097-
620 0010(199607)71:3<313::AID-JSFA586>3.0.CO;2-N

López-Maestresalas, A., Aernouts, B., van Beers, R., Arazuri, S., Jarén, C., de Baerdemaeker, J., & Saeys, W. (2015). Bulk Optical Properties of Potato Flesh in the 500–1900 nm Range. *Food and Bioprocess Technology*, 9(3), 463–470. doi:10.1007/s11947-015-1639-0

Lu, R. (2004). Multispectral imaging for predicting firmness and soluble solids content of apple fruit. *Postharvest Biology and Technology*, *31*(2), 147–157. doi:10.1016/j.postharvbio.2003.08.006

Lu, R., Cen, H., Huang, M., & Ariana, D. P. (2010). Spectral Absorption and Scattering Properties of Normal Bruised Apple Tissue. *Transactions of the ASABE*, *53*(1), 263–269.

McGlone, V. A., Jordan, R. B., & Martinsen, P. J. (2002). Vis/NIR estimation at harvest of pre- and post-storage quality indices for “Royal Gala” apple. *Postharvest Biology and Technology*, *25*(2), 135–144. doi:10.1016/S0925-5214(01)00180-6

Merzlyak, M. N., Solovchenko, A. E., & Gitelson, A. A. (2003). Reflectance spectral features and non-destructive estimation of chlorophyll, carotenoid and anthocyanin content in apple fruit. *Postharvest Biology and Technology*, *27*(2), 197–211. doi:10.1016/S0925-5214(02)00066-2

Mir, N. a, Curell, E., Khan, N., Whitaker, M., & Beaudry, R. M. (2001). Harvest Maturity , Storage Temperature , and 1-MCP Application Frequency Alter Firmness Retention and Chlorophyll Fluorescence of “ Redchief Delicious ” Apples. *J. Amer. Soc. Hort. Sci.*, *126*(5), 618–624.

Nguyen Do Trong, N., Erkinbaev, C., Tsuta, M., De Baerdemaeker, J., Nicolaï, B., & Saeys, W. (2014). Spatially resolved diffuse reflectance in the visible and near-infrared wavelength range for non-destructive quality assessment of “Braeburn” apples. *Postharvest Biology and Technology*, *91*, 39–48. doi:10.1016/j.postharvbio.2013.12.004

Nicolaï, B. M., Defraeye, T., De Ketelaere, B., Herremans, E., Hertog, M. L. a T. M., Saeys, W., Torricelli, A., Vandendriessche, T., & Verboven, P. (2014). Nondestructive measurement of fruit and vegetable quality. *Annual Review of Food Science and Technology*, *5*, 285–312. doi:10.1146/annurev-food-030713-092410

Peirs, A., Lammertyn, J., Ooms, K., & Nicolaï, B. M. (2001). Prediction of the optimal picking date of different apple cultivars by means of VIS/NIR-spectroscopy. *Postharvest Biology and Technology*, *21*(2), 189–199. doi:10.1016/S0925-5214(00)00145-9

Peirs, A., Scheerlinck, N., Berna Perez, A., Jancsók, P., & Nicolaï, B. M. (2002). Uncertainty analysis and modelling of the starch index during apple fruit maturation. *Postharvest Biology and Technology*, *26*(2), 199–207. doi:10.1016/S0925-5214(02)00038-8

Peirs, A., Schenk, A., & Nicolaï, B. M. (2005). Effect of natural variability among apples on the accuracy of VIS-NIR calibration models for optimal harvest date predictions. *Postharvest Biology and Technology*, *35*(1), 1–13. doi:10.1016/j.postharvbio.2004.05.010

Prahl, S. A., van Gemert, M. J. C., & Welch, A. J. (1993). Determining the optical properties of turbid mediaby using the adding-doubling method. *Applied Optics*, *32*(4), 559–568. doi:10.1364/AO.32.000559

661 Qin, J., & Lu, R. (2008). Measurement of the optical properties of fruits and vegetables using
662 spatially resolved hyperspectral diffuse reflectance imaging technique. *Postharvest Biology*
663 *and Technology*, *49*(3), 355–365. doi:10.1016/j.postharvbio.2008.03.010

664 Qin, J., & Lu, R. (2009). Monte Carlo simulation for quantification of light transport features in
665 apples. *Computers and Electronics in Agriculture*, *68*(1), 44–51.
666 doi:10.1016/j.compag.2009.04.002

667 Qin, J., Lu, R., & Peng, Y. (2009). Prediction of apple internal quality using spectral
668 absorption and scattering properties, *52*(2), 499–507.

669 Reay, P. F., Fletcher, R. H., & Thomas, V. J. G. (1998). Chlorophylls, carotenoids and
670 anthocyanin concentrations in the skin of “Gala” apples during maturation and the influence
671 of foliar applications of nitrogen and magnesium. *Journal of the Science of Food and*
672 *Agriculture*, *76*, 63–71. doi:10.1002/(SICI)1097-0010(199801)76:1<63::AID-
673 JSFA908>3.0.CO;2-K

674 Rowe, P. I., Künnemeyer, R., McGlone, A., Talele, S., Martinsen, P., & Seelye, R. (2014).
675 Relationship between tissue firmness and optical properties of “Royal Gala” apples from 400
676 to 1050nm. *Postharvest Biology and Technology*, *94*, 89–96.

677 Rutkowski, K. P., Michalczuk, B., & Konopacki, P. (2008). NONDESTRUCTIVE
678 DETERMINATION OF “GOLDEN DELICIOUS ” APPLE QUALITY AND HARVEST
679 MATURITY. *Journal of Fruit and Ornamental Plant Research*, *16*, 39–52.

680 Saeys, W., Velazco-Roa, M. a, Thennadil, S. N., Ramon, H., & Nicolaï, B. M. (2008). Optical
681 properties of apple skin and flesh in the wavelength range from 350 to 2200 nm. *Applied*
682 *Optics*, *47*(7), 908–19.

683 Schotsmans, W., Verlinden, B. E., Lammertyn, J., & Nicolaï, B. M. (2004). The relationship
684 between gas transport properties and the histology of apple. *Journal of the Science of Food*
685 *and Agriculture*, *84*(10), 1131–1140. doi:10.1002/jsfa.1768

686 Seifert, B., Zude, M., Spinelli, L., & Torricelli, A. (2014). Optical properties of developing pip
687 and stone fruit reveal underlying structural changes. *Physiologia Plantarum*, (153), 327–336.
688 doi:10.1111/ppl.12232

689 Singha, S., Baugher, T. a, Townsend, E. C., & D’Souza, M. C. (1991). Anthocyanin
690 Distribution in `Delicious’ Apples and the Relationship between Anthocyanin Concentration
691 and Chromaticity Values. *Journal of the American Society for Horticultural Science*, *116*(3),
692 497–499.

693 Smith, A. M., Zeeman, S. C., & Smith, S. M. (2005). Starch Degradation. Annual Review of
694 Plant Biology, 56(1), 73–98. doi:10.1146/annurev.arplant.56.032604.144257

695 Solovchenko, A., & Merzlyak, M. (2003). Optical properties and contribution of cuticle to UV
696 protection in plants: experiments with apple fruit. *Photochemical & Photobiological Sciences :*
697 *Official Journal of the European Photochemistry Association and the European Society for*
698 *Photobiology*, *2*(8), 861–866. doi:10.1039/b302478d

699 Song, J., Deng, W., Beaudry, R. M., & Armstrong, P. R. (1997). Changes in Chlorophyll
700 Fluorescence of Apple Fruit during Maturation, Ripening, and Senescence. *HortScience*,
701 *32*(5), 891–896.

Stevenson, D., Domoto, P., & Jane, J. (2006). Structures and functional properties of apple (Malus domestica Borkh) fruit starch. *Carbohydrate Polymers*, *63*(3), 432–441. doi:10.1016/j.carbpol.2005.10.009

Streif, J. (1996). Optimum harvest date for different apple cultivars in the “Bodensee” area. In A. de Jager & D. Johnson (Eds.), *The Postharvest Treatment of Fruit and Vegetables: Determination and Prediction of Optimum Harvest Date of Apple and Pears. COST 94* (pp. 15–20). Brussels, Belgium.

Torricelli, A., Spinelli, L., Vanoli, M., Leitner, M., Nemeth, A., Nguyen Do Trong, N., Nicolaï, B., & Saeys, W. (2013). *Optical coherence tomography (OCT), space-resolved reflectance spectroscopy (SRS) and time-resolved reflectance spectroscopy (TRS): principles and applications to food microstructures*. Elsevier. doi:10.1533/9780857098894.1.132

Tuchin, V. (2007). Methods and algorithms for the measurements of optical parameters of tissues. In *Tissue Optics* (Second Edi., pp. 143–256). Bellingham, WA: SPIE Press.

Van Beers, R., Aernouts, B., León Gutiérrez, L., Erkinbaev, C., Rutten, K., Schenk, A., Nicolaï, B., & Saeys, W. (2015). Optimal Illumination-Detection Distance and Detector Size for Predicting Braeburn Apple Maturity from Vis/NIR Laser Reflectance Measurements. *Food and Bioprocess Technology*, *8*(10), 2123–2136. doi:10.1007/s11947-015-1562-4

Veraverbeke, E. A., Lammertyn, J., Nicolaï, B. M., & Irudayaraj, J. (2005). Spectroscopic evaluation of the surface quality of apple. Journal of Agricultural and Food Chemistry, 53(4), 1046–1051. doi:10.1021/jf0486848

Verboven, P., Kerckhofs, G., Mebatsion, H. K., Ho, Q. T., Temst, K., Wevers, M., Cloetens, P., & Nicolaï, B. M. (2008). Three-dimensional gas exchange pathways in pome fruit characterized by synchrotron x-ray computed tomography. *Plant Physiology*, *147*(June), 518–527. doi:10.1104/pp.108.118935

Verboven, P., Nemeth, A., Abera, M. K., Bongaers, E., Daelemans, D., Estrade, P., Herremans, E., Hertog, M., Saeys, W., Vanstreels, E., Verlinden, B., Leitner, M., & Nicolaï, B. (2013). Optical coherence tomography visualizes microstructure of apple peel. *Postharvest Biology and Technology*, *78*, 123–132.

Watté, R., Aernouts, B., Van Beers, R., Herremans, E., Ho, Q. T., Verboven, P., Nicolaï, B., & Saeys, W. (2015). Modeling the propagation of light in realistic tissue structures with MMC-fpf: a meshed Monte Carlo method with free phase function. *Optics Express*, *23*(13), 17467. doi:10.1364/OE.23.017467

Watté, R., Aernouts, B., Van Beers, R., & Saeys, W. (2015). Robust metamodel-based inverse estimation of bulk optical properties of turbid media from spatially resolved diffuse reflectance measurements. *Optics Express*, *5*(11), 27880–27898. doi:10.1364/OME.5.0027880

Zamora-Rojas, E., Aernouts, B., Garrido-Varo, A., Pérez-Marín, D., Guerrero-Ginel, J. E., & Saeys, W. (2013). Double integrating sphere measurements for estimating optical properties of pig subcutaneous adipose tissue. *Innovative Food Science & Emerging Technologies*, *19*, 218–226.